

Plasma Heating Due to Cyclic Diffusion Across a Separatrix

F. Anderegg, M. Affolter, D.H.E.Dubin, and C.F. Driscoll

University of California San Diego, Physics Department 0319, La Jolla, CA 92093, USA

(Dated: April 18, 2018)

We observe plasma heating due to collisional diffusion across a separatrix when a pure ion plasma column is pushed back and forth across a partial trapping barrier. The barrier is an externally applied axisymmetric “squeeze” potential, which creates a velocity separatrix between trapped and passing particles. Weak collisions then cause separatrix crossings, leading to irreversible heating. The heating rate scales as the square root of the oscillation rate times the collision frequency, and thus is large for low-collisionality fusion plasmas. The particle velocity distribution function is measured with coherent Laser Induced Fluorescence, and shows passing and trapped particles having an out-of-phase response to the forced plasma oscillations. “Synthetic” collisions from externally applied electrostatic noise cause velocity diffusion and enhanced separatrix crossings, with resultant heating also scaling as square root of the synthetic collisions rate.

Electric and magnetic field inhomogeneities in plasmas can create collisional boundary layers between trapped and passing particles. These boundary layers are predicted to enhance plasma transport [1, 2], dissipate poloidal rotation [3], and damp waves [4, 5]. Experiments, numerical simulations, and theories on tokamaks [6, 7], stellarators [8, 9], and pure electron plasmas [10–14] have shown increased transport and wave damping resulting from applied field inhomogeneities. However, prior experiments have not directly observed the signature $\sqrt{\nu_c f}$ scaling of these boundary layer analyses, where ν_c is the collisionality and f is the frequency of the particle forcing.

A heating rate proportional to $\sqrt{\nu_c f}$ is similar to the viscous heating of a sheared fluid caused by an oscillating plate [15, 16]. Here, oscillating untrapped plasma takes the place of the plate, transferring energy and momentum diffusively into the trapped plasma through a boundary layer of width proportional to $\sqrt{\nu_c/f}$, as in the classic fluid problem.

In this letter, we present quantitative measurements of the particle dynamics in the presence of a velocity separatrix, and the resulting plasma heating induced by collisional diffusion across this separatrix. Trapped and passing particle populations are created by applying a cylindrically-symmetric electrostatic squeeze near the middle of a pure ion plasma column. When the plasma is sinusoidally forced through this potential barrier, the trapped and passing particles experience different dynamics, forming a collisional boundary layer. The particle dynamics are directly measured using a coherent Laser Induced Fluorescence technique, and the trapped (passing) particles are observed to move in (out-of)-phase with the applied forcing, in quantitative agreement with a recent collisionless adiabatic invariant analysis [17].

Ion-ion collisions cause velocity diffusion and separatrix crossings, which leads to irreversible heating scaling as $\dot{T}/T \propto \sqrt{\nu_c f} V_{sqz}^2 \delta L^2$ where δL is the size of the forced oscillation through the squeeze potential V_{sqz} . This heating is in quantitative agreement with recent theory [17]. These experiments for the first time confirm the signature $\sqrt{\nu_c f}$ scaling of the heating by changing

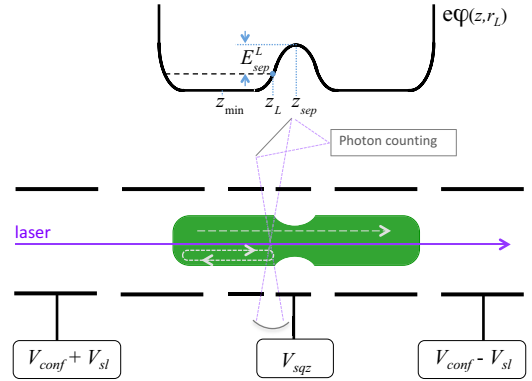


FIG. 1. Pure ion plasma in Penning-Malmberg trap forced through “squeeze” with oscillating voltage V_{sl} . The figure shows the plasma pushed to the right, defined as phase 0° . Top curve sketches potential along the magnetic field at the laser radial position.

the rate f at which the plasma is oscillated through the squeeze, and by enhancing the effective collisionality ν_{eff} through enhanced velocity diffusion from externally applied noise.

A Penning-Malmberg trap with a wall radius $R_W = 2.86\text{cm}$ is used to confine these un-neutralized Magnesium ion plasmas in a magnetic field of $B = 3$ Tesla [18], as shown in Figure 1. Using Laser Induced Fluorescence diagnostics, the plasma radial density profile $n(r, z_L)$ is measured at the laser location z_L , and the 2D density $n(r, z)$ is calculated using a Boltzmann-Poisson solver [19]. A typical plasma, axially confined with $V_{conf} = 100\text{V}$, has a length $L_p \simeq 11\text{cm}$, and a radially uniform density $n_0 \simeq 2 \times 10^7 \text{cm}^{-3}$ out to $R_p \simeq 0.5 \text{cm}$, resulting in an almost rigid $E \times B$ plasma rotation at a frequency $f_{E \times B} \simeq 10 \text{kHz}$. The ions are cooled to 0.04eV by collision with neutral H_2 at a pressure $P \simeq 10^{-8} \text{Torr}$, and cyclotron heating on the $^{24}\text{Mg}^+$ ions controls the plasma temperature over the range $0.04 \text{eV} < T < 1 \text{eV}$. The plasma is confined in steady state with the use of weak “rotating-wall” electric potentials [20].

For these experiments, a velocity separatrix is created by applying a squeeze potential V_{sqz} to an annular electrode as shown in Figure 1, and a cyclic axial plasma flow (sloshing) is formed by adding nominally sinusoidal voltages $\pm V_{sl} \cos(2\pi f_{sl} t)$ to the end confinement voltages V_{conf} , with the \pm referring to left/right ends. Typically, the slosh amplitude $V_{sl} \simeq 50V_p$ effectively displaces each end a distance $\pm \delta L \approx 0.5$ cm.

To test recent theory [17], these experiments are performed in the “super-banana” regime defined by $\nu_c \ll 2\pi f_{sl} \ll 2\pi f_b$ [8, 17], where f_{sl} is the slosh frequency and f_b is the axial bounce frequency. The sloshing frequency is typically $f_{sl} = 500$ Hz, which is large compared to the classical ion-ion collision rate given by $\nu_c = \frac{8}{15} \sqrt{\pi} n \bar{v} b^2 \ln(r_c/b) \simeq 0.5s^{-1} (n/10^7 \text{cm}^{-3}) (T_{eV}/1\text{eV})^{-3/2}$, so that bulk viscous heating scaling as ν_c/f_{sl} is weak [21]. Also f_{sl} is small compared to the thermal $^{24}\text{Mg}^+$ ion bounce frequency $f_b = \bar{v}/2L_p \simeq 10\text{kHz} (10\text{cm}/L_p) (T/1\text{eV})^{1/2}$ with $\bar{v} = 2. \times 10^5 (T/1\text{eV})^{1/2}$ cm/s, so that the ν_c – independent heating due to excitation of Landau resonances is suppressed [22].

The particle dynamics are measured using a coherent Laser Induced Fluorescence (LIF) technique [23], which measures the parallel velocity distribution function $F(v, z_L)$ coherent with the phase $\theta(t)$ of the forced plasma sloshing. These coherent distribution are measured by tuning the laser wavelength to be resonant with a Mg^+ ion moving at velocity v . The plasma is then sinusoidally forced through the separatrix V_{sqz} for 500ms (250 cycles at 500Hz) and the time of arrival of each fluorescent photon is recorded along with the phase of the slosh. The plasma is then allowed to re-equilibrate for 10 seconds, and the process is repeated for 100 different laser wavelengths, encompassing the entire particle velocity distribution.

Post-processing of the data arranges the photons from each wavelength (velocity) into 16 phase bins corresponding to the phase of the forced oscillations $\theta_j = j2\pi/16$, and the entire phase-coherent distribution is reconstructed as $F(v, \theta_j, z_L)$. Due to the finite size of the laser beam and viewing volume, these measurement are convolved over a 0.2cm diameter, 0.3cm long cylinder centered at z_L . The beam diameter was selected to optimized the signal to noise and minimize non-linear distortion of the distribution function.

Figure 2a shows the coherent $F(v, \theta_j, z_L)$, obtained from 125 slosh cycles, at two phases corresponding to the right (phase 0°) and left (phase 180°) slosh extremes. For phase 0° (red dots), the plasma is being forced to the right as shown in figure 1. Therefore, the trapped particles at the laser location z_L are compressed, which increases the density of particles at low velocity. In contrast, the density of passing particles at z_L decreases to equalize the potential along on a given field line. For phase 180° (blue triangles) the plasma is forced to the left, and density changes are reversed. The dotted line of

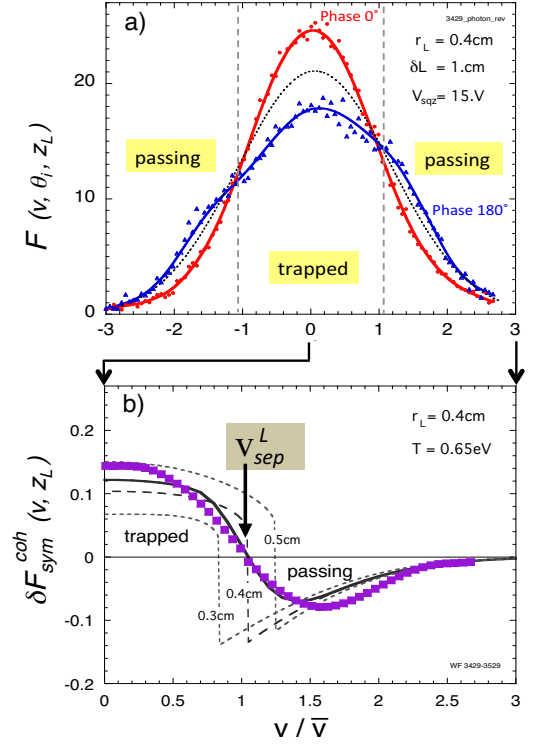


FIG. 2. a) Measured velocity distribution shown for phase 0° (plasma pushed to the right) and phase 180° (plasma pushed to the left). b) Symmetric coherent response of the velocity distribution. Both are plotted versus normalized particle velocity.

figure 2a is the average Maxwellian distribution $F_M(v)$, and the two vertical grey dashed lines indicate the minimum particle velocity v_{sep}^L at the laser location required to cross the separatrix.

We also observe that the entire distribution of particles is sloshing at a low velocity. For the data presented in figure 2a, $v_{sl} \simeq 5000$ cm/s $\simeq 0.03\bar{v}$ is measurable but too small to be visible on this plot. Assuming a forced sinusoidal oscillation of the plasma, the complex coherent change of the distribution is

$$\delta F^{coh}(v) \equiv \sum_{j=0}^{15} F(v, \theta_j) \times [\cos\theta_j + i \sin\theta_j], \quad (1)$$

where $\theta_j = j2\pi/16$ are the phase bins. Changes in the plasma density and temperature appear in the v –symmetric response given by

$$\delta F_{sym}^{coh}(v) \equiv \frac{1}{2F_M(0)} [\delta F^{coh}(v) + \delta F^{coh}(-v)], \quad (2)$$

where F_M is the average Maxwellian distribution. The anti-symmetric response yields the fluid velocity of the particles.

The symmetric coherent response $\delta F_{sym}^{coh}(v, z_L)$ is plotted in figure 2b. The horizontal axis is the measured par-

ticle velocity at z_L , normalized to the initial thermal velocity $\bar{v} = 1.6 \times 10^5$ cm/s from temperature $T = 0.65$ eV. Each symbol corresponds to measurements performed at two wavelengths of the laser, corresponding to $\pm v$. The collision rate is $\nu_c = 2$ sec $^{-1}$, so a thermal ion experiences about 1 momentum-transfer collisions during the 250 slosh cycles. The symmetric response $\delta F_{sym}^{coh}(v)$ clearly shows that the trapped particles ($v < 1.05 \bar{v}$) are in-phase with the forcing, whereas the passing particles ($v > 1.05 \bar{v}$) are out-of-phase. At phase 0° (sloshed right), the left-trapped density increases while the passing particle in the left density decreases. The velocity where $\delta F_{sym}^{coh}(v) = 0$ is the measured separatrix velocity v_{sep}^L at the laser location.

The curves of Figure 2b are the theory predicted $\delta F_{sym}^{coh}(v, z_L, r_L)$. This theory first evaluates the collisionless adiabatic response to the $\cos(2\pi f_{sl} t)$ oscillation in the external potential. Assuming the variations are small, so linear theory can be applied, the perturbed distribution is

$$\delta F(z, v_z, r, t) = -\cos(2\pi f_{sl} t) \frac{e \delta \varphi(z, r) - e \langle \delta \varphi \rangle(r, E)}{T}, \quad (3)$$

where the angle brackets indicate a “bounce-average” over a collisionless particle orbit, $E(z, v_z, r) = e\varphi + \frac{1}{2}mv_z^2$ is the energy of a particle, and $\delta \varphi(z, r) \cos(2\pi f_{sl} t)$ is the perturbed electrostatic potential. The particle dynamics is at fixed r , but the potentials $\varphi(z, r)$ and $\delta \varphi(r, z)$ are determined by self-consistent solution of Poisson’s equation with the wall boundary conditions. Thus, the separatrix energy $E_{sep}(z, r)$ depends strongly on r , and passing particles will “shield” the potential from trapped particles at other radii.

The long dashed-line of figure 2b is the collisionless theory prediction of $\delta F_{sym}^{coh}(v)$ for $r = 0.4$ cm with a sharp discontinuity at the separatrix. The discontinuity is due to the bounce average of $\delta \varphi$ being different for trapped particle and passing particles. The short dashed-lines are the theory predictions for $r = 0.3$ cm and $r = 0.5$ cm corresponding to the edges of the laser beam. The solid line is the prediction of $\delta F_{sym}^{coh}(v)$ averaged over the laser beam, predicting a smooth laser measured distribution. Data with an increased beam size (not shown) corroborates the effect of spatial averaging.

The particle kinetic energy required to pass through the squeeze is a function of z -position and radius in the plasma, and we measure $E_{sep}^L(z_L, r_L) \equiv \frac{1}{2}m[v_{sep}^L(z_L, r_L)]^2$ by detecting the change of sign in the symmetric response of $\delta F_{sym}^{coh}(v)$ occurring at v_{sep}^L . Note that the LIF measures the kinetic energy of particles only at $z = z_L$, so particles with energy less than $\varphi(z_L, r)$ are not detected since they do not have enough energy to reach the diagnostic location. On axis $r = 0$, at z_{min} , the potential with respect to the trap wall is $e\varphi(z_{min}, r = 0) = 14.89$ eV, at the laser location the $e\varphi(z_L, r = 0) = 14.98$ eV, and $e\varphi(z_{sep}, r = 0) = 15.114$ eV so the separatrix energy relative to the laser position is $E_{sep}^L \equiv e\varphi(z_{sep}, r = 0) - e\varphi(z_L, r = 0) = 0.134$ eV.

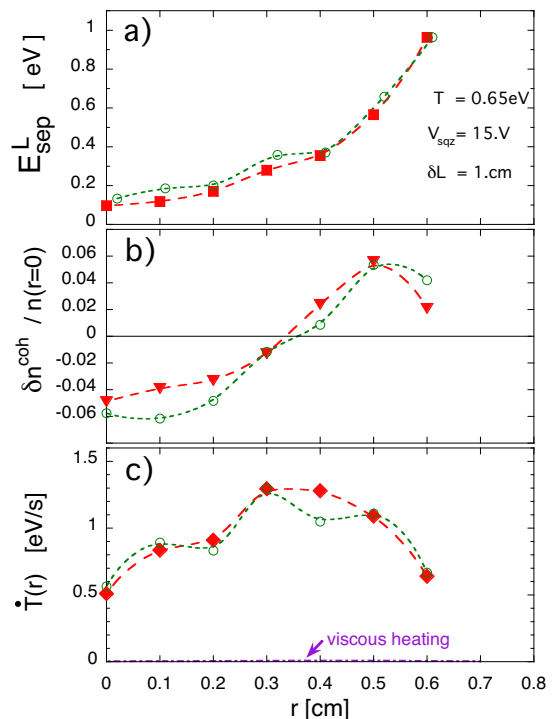


FIG. 3. Radial profile at “laser location” z_L of a) Kinetic particle energy required to cross separatrix, b) coherent density perturbation, and c) heating rate \dot{T} plotted against radius. Solid symbol are experimental measurement and open symbols are theory predictions.

Figure 3a plots the measured E_{sep}^L (squares) and theory prediction calculated from Boltzmann-Poisson equilibrium $e\varphi(z, r)$ (open circles) as a function of radius. Figure 3a shows that the applied squeeze potential is Debye shielded by the plasma, reducing the separatrix energy in the center. Measurements at all seven radial locations are performed on the same plasma, but due to repeated sloshing through the squeeze potential some particles on the outside edge of the plasma are lost. The plasma radius evolves from 0.64cm to 0.57cm over the course of the measurement. The data are collected at “interlaced” radii to avoid systematic drift. The theory predictions of figure 3 are calculated at each specific radius for the measured experimental conditions. The lines on figure 3 are merely to guide the eye.

Integrating $\delta F_{sym}^{coh}(v, r)$ gives the density perturbation $\delta n^{coh}(r)$ plotted versus radius in figure 3b (triangles), with the theory prediction (open circles). At small radii, δn is negative corresponding to Debye shielding with negligible trapping. In contrast, at large radii more particles are trapped, and δn is positive. At $r \simeq 0.32$ cm, $\delta n^{coh} \simeq 0$ indicating that about half of the particles are trapped.

The second half of this letter focuses on the plasma heating caused by collisions acting on this particle dynamics. As the trapped particles are compressed/expanded by the slosh, they undergo an adia-

batic change in temperature $\delta T = \pm 2T (\delta L/L)^2$ every period of the slosh oscillation, where the \pm indicates that δT reverses sign across the separatrix. A small fraction of trapped particles within the collisional boundary layer of energy width $\Delta E = \sqrt{T e\varphi_s \nu_c / (2\pi f_{sl})}$ around the separatrix energy $e\varphi_s$ can collisionally cross the separatrix. These particles become passing and are then retrapped on either side of the separatrix within one oscillation period. This makes the adiabatic heating of the trapped particles irreversible, which leads to plasma heating scaling as $f_{sl} (e\varphi_s)^2 (\delta L/L)^2 \alpha_{BL}$, where α_{BL} is the fraction of particles in the boundary layer. For a Maxwellian distribution, $\alpha_{BL} \sim (\Delta E / \sqrt{T e\varphi_s}) \exp(-e\varphi_s/T)$, so the heating rate is

$$\frac{\dot{T}}{T} \sim \sqrt{\nu_c f_{sl}} (e\varphi_s/T)^2 (\delta L/L)^2 \exp(-e\varphi_s/T). \quad (4)$$

The exact expression for the heating rate can be found in equation 51 of reference [17], and was used to calculate the open circles of Figure 3c for each radius. Theory and experiment are in quantitative agreement at each radius, and show that the maximum heating occurs where about half the particles are trapped. Note that theory generally describes the heating per cycle scaling as $\sqrt{\nu_c / f_{sl}}$. Experimentally we measure the heating rate (per unit of time) that scales as $f_{sl} \sqrt{\nu_c / f_{sl}} = \sqrt{\nu_c f_{sl}}$.

In these experiments $e\varphi_s/T \ll 1$, and we observe a heating rate with the $V_{sqz}^2 \delta L^2$ scaling of Eq.4 over the range $3 < V_s < 15V$ and $0.35cm < \delta L < 1.8cm$. We also for the first time observe the $\sqrt{\nu_c f_{sl}}$ heating rate characteristic of boundary layer analysis. Figure 4 shows the normalized heating rate \dot{T}/T for a high collisionality plasma ($\nu_c \simeq 110.s^{-1}$) plotted with triangles ($\delta L = 1.cm$) against the slosh frequency multiplied by the collision rate $f_{sl} \nu_c$ for a squeeze voltage $V_{sqz} = 7V$. The heating rate is measured at a laser radial location $r_L = 0.5cm$, and is normalized by the square of the amplitude of the sloshing. A second sloshing amplitude ($\delta L = 1.8cm$) is also shown with diamonds on figure 4. The blue triangles and diamonds show that over a range of ~ 25 in sloshing frequency ($50Hz < f_{sl} < 1200Hz$), the heating rate scales as $\sqrt{\nu_c f_{sl}}$, as expected from the theory model of particles crossing the separatrix. The solid line is the heating rate predicted by theory from equation 51 of reference [17]. Also plotted, with a green square, is the normalized heating rate for the low collisionality plasma ($\nu_c \simeq 2.s^{-1}$) of figure 2 and 3 at $r_L = 0.5cm$.

To verify the collisional nature of the separatrix crossing, we introduce ‘‘synthetic collisions’’ by adding at one end of the trap a weak ‘‘white noise’’ to the sloshing voltage ($f_{sl} = 500Hz$). The frequency of the noise f_{noise} is less than 20kHz to avoid exciting plasma waves. The small ‘‘noise’’ perturbation enhances velocity diffusion and increases the heating rate significantly. We also measure the heating rate due to the noise alone and subtract it from the total heating rate to obtain the ‘‘noise’’ – enhanced heating rate \dot{T}_{enh} . We determine the effective synthetic collision rate from the temperature

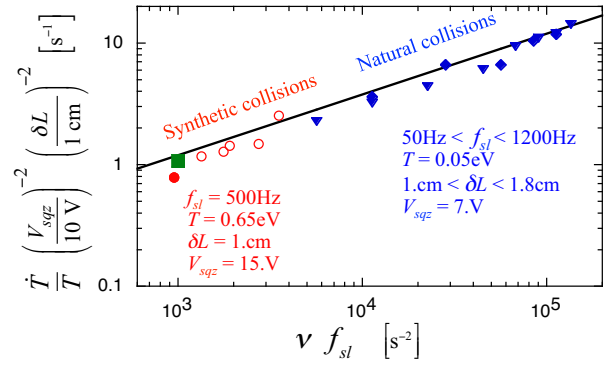


FIG. 4. Normalized heating rate \dot{T}/T plotted versus collision rate times sloshing frequency showing heating rate proportional to $\sqrt{\nu f_{sl}}$. The solid blue symbols are from various f_{sl} and the open symbols are from added synthetic collision to a low collisionality plasma (red dot). The green square is the plasma used for figure 2 and 3.

evolution in presence of the noise perturbation only as $\nu_{eff} \equiv \frac{3}{2} \dot{T}/T_0$. The solid circle in 4 is from a low collisionality plasma with no added noise onto which artificial collision are added. The enhanced heating rate (\dot{T}_{enh}/T) is plotted against the total collision rate ($\nu = \nu_c + \nu_{eff}$) times the slosh frequency in figure 4 with open circle. Here synthetic collisions forcing particle to cross the separatrix result in the same scaling $\sqrt{\nu f_{sl}}$ as ‘‘natural’’ collisions inducing separatrix crossing.

Experimentally, it is worth noting that oscillating the plasma in the absence of a separatrix, produces negligible heating. Furthermore, using a negative squeeze voltage does not produce separatrix heating, since it does not create a separatrix between separate trapped populations. For example applying $V_{sqz} = -15V$ on a plasma similar to the one used in figure 2 and 3 results in a negligible heating rate $\dot{T} \simeq 0.02eV/s$ at $r_L = 0.4cm$.

Other mechanisms can also heat the plasma, albeit at a much slower rate when $\nu_c \ll 2\pi f_{sl}$. For instance, plasma compressions cause $T_{\parallel} \neq T_{\perp}$, and their subsequent collisional relaxation causes irreversible bulk viscous heating of order $\nu_c T (\delta L/L)^2$ [21]. Here the trapped particles are also compressed and expanded producing bulk viscous heating proportional to ν_c^2 . For the plasma data of figure 3 this heating is maximum at $r = 0.42 cm$ where $\dot{T}_{vis} = 0.009 eV/s$ about 100 times smaller that the measured heating due to particle crossing the separatrix, as shown by the dotted line at the bottom of the graph.

Also, ν_c -independent [22] heating can occur due to Landau resonances at $f = n f_b(E)$, $n = 1, 2, \dots$, (where $f_b(E)$ is the energy-dependent bounce frequency), but such resonances are suppressed here since we choose f_{sl} small compared to the mean thermal bounce frequency f_b .

To summarize, we have used external electrodes to create a controlled velocity space separatrix, and have forced the plasma to oscillate through it at frequencies in the super-banana regime $\nu_c \ll 2\pi f_{sl} \ll 2\pi f_b$. We experi-

mentally identify passing and trapped particles, and have observed directly the coherent particle response in quantitative agreement with newly developed theory. Furthermore we measure plasma heating scaling as $\sqrt{\nu_c f_{sl}}$, $(\delta L/L_p)^2$ and V_s^2 , in quantitative agreement with superbanana heating due to particle diffusively crossing an en-

ergy separatrix.

ACKNOWLEDGMENTS

This work was supported by National Science Foundation Grant PHY-1414570, Department of Energy Grant DE-SC0002451 and Department of Energy High Energy Density Laboratory Plasma Grant DE-SC0008693.

-
- [1] A. A. Galeev, R.Z. Sagdeev, H.P. Furth, M.N. Rosenbluth, *Phys. Rev. Lett.* **22**, 511 (1969)
 - [2] K.C. Shaing, P. Cahyna, M. Becoulet, J.-K. Park, S.A. Sabbagh, M.S. Chu, *Physics of Plasmas* **15**, 082506 (2003)
 - [3] R.C. Morris, M.G. Haines, R.J. Hastie, *Physics of Plasmas* **3**, 4513 (1996)
 - [4] T.J. Hilsabeck, A.A. Kabantsev, C.F. Driscoll, T.M.O’Neil, *Phys. Rev. Lett.* **90**, 245002 (2003)
 - [5] M.N. Rosenbluth, D.W. Ross, D.P. Kostomarov, *Nuclear Fusion* **12**, 3 (1972)
 - [6] W. Zhu, S.A. Sabbagh, R.E. Bell, J.M. Bialek, M.G. Bell, B.P. LeBlanc, S.M. Kaye, F.M. Levinton, J.E. Menard, K.C. Shaing, A.C. Sontag, H. Yuh, *Phys. Rev. Lett.* **96**, 225002, (2006)
 - [7] B. LaBombard et al., *Nuclear Fusion* **40**, 2041 (2000)
 - [8] H. Mynick, *Phys. Plasmas* **13**, 058102 (2006).
 - [9] J.M. Faustin, W.A. Copper, J.P. Graves, D. Pfefferle and J. Geiger, *Nuclear Fusion* **56**, 092006 (2016).
 - [10] A.A. Kabantsev and C.F. Driscoll, *Phys. Rev. Lett.* **97**, 095001 (2006)
 - [11] A.A. Kabantsev, D.H.E. Dubin, C.F. Driscoll, Y.A. Tsidulko, *Phys. Rev. Lett.* **105**, 205001 (2010)
 - [12] A.A. Kabantsev C.F. Driscoll, *Phys.Rev. Lett.* **112**, 055003 (2014)
 - [13] C.F. Driscoll, A.A. Kabantsev, D.H.E. Dubin, Y.A. Tsidulko, AIP Conference Proceedings 1521, page 15-25 (2013), edited by X. Sarasola, L. Schweikhard, T.S. Pedersen.
 - [14] J. Fajans, *Physics of Plasmas* **10**, 1209 (2003)
 - [15] G.K. Batchelor, “Hydrodynamics”, 6th edition, §345 Cambridge University Press, Cambridge, (1932).
 - [16] H. Lamb, “An Introduction to Fluid Dynamics”, Cambridge University Press, Cambridge, (1967).
 - [17] D.H.E. Dubin, *Physics of Plasmas*, **24**, 112120(2017)
 - [18] F. Anderegg, X.-P. Huang, E. Sarid, and C.F. Driscoll, *Rev. Sci. Instrum.* **68**, 2367 (1997)
 - [19] E.H. Chao, R.C. Davidson, S.F. Paul, K.S. Fine, Non-Neutral Plasma Physics III, AIP Conference Proceedings 498, page 461-468, (1999), edited by J.J. Bollinger, R.L. Spencer, R.C. Davidson
 - [20] X.-P. Huang, F. Anderegg, E.M. Hollmann, C.F. Driscoll and T.M. O’Neil, *Phys. Rev. Lett.* **78**, 875 (1997); E.M. Hollmann, F. Anderegg, and C.F. Driscoll, *Phys. Plasmas* **7**, 2776 (2000)
 - [21] B.P. Cluggish, J.R. Danielson, and C.F. Driscoll, *Phys. Rev. Lett.* **81**, 353 (1998)
 - [22] F. Anderegg, M. Affolter, A. Kabantsev, D.H.E. Dubin, A. Ashourvan, and C.F. Driscoll, *Physics of Plasma* **23**, 055706 (2016)
 - [23] F. Anderegg, C.F. Driscoll, D.H.E. Dubin, and T.M. O’Neil, *Phys. Rev. Lett.* **102**, 095001 (2009)